Supplementary material for: **Synorogenic extension localized by upper-crustal thickening: An example from the Late Cretaceous Nevadaplano**

Section SM1: Thermochronology sample information

Twelve quartzite samples were collected from the map area (Table SM1), six from the Lower Cambrian Prospect Mountain Quartzite in the footwall of the Hoosac fault system and Dugout Tunnel fault, four from the Middle Ordovician Eureka Quartzite in the footwall of the Reese and Berry detachment system, and two from the basal quartzite of the Lower Devonian Beacon Peak Dolomite in the footwall of the Pinto Summit fault. Minerals were separated at Apatite to Zircon, Inc., using standard crushing, magnetic and heavy liquid separation techniques. Zircons were obtained from all 12 samples, but apatite of sufficient quantity were only obtained from samples 02SL10 and 06SL11.

Table SM1: Eureka thermochronology samples and cooling ages.

Sample	Latitude (dd.ddddd)	Longitude (dd.ddddd)	Elevation (m)	Map unit	Lithology	Footwall of structure	ZFT age (Ma)	ZFT 1σ error (Ma)	# of zircons analyzed	ZHe age (Ma)	ZHe 2σ error (Ma)	# of zircons analyzed	AFT age (Ma)	AFT 1σ error (Ma)	# of apatites analyzed	AHe age (Ma)	AHe 2σ error (Ma)	# of apatites analyzed
01SL10	39.44272	116.00317	2750	Cpm[1]	quartzite	HFS and DTF	72.5	4.5	16	72.57	1.26	3	-	-	-	-	-	-
02SL10	39.45036	115.99856	2890	Cpm[1]	quartzite	HFS and DTF	460.5	36.6	10	81.50	1.90	2	52.6	7.0	7	28.82	0.92	2
06SL11	39.45692	116.00181	2685	Cpm[1]	quartzite	HFS and DTF	75.0	5.5	20	305.6	6.2	2	41.8	3.7	19	-	-	-
07SL11	39.46061	116.00611	2420	Cpm[1]	quartzite	HFS and DTF	77.6	5.1	20	63.20	1.06	3	-	-	-	-	-	-
01SL12	39.44261	116.00575	2755	Cpm[1]	quartzite	HFS and DTF	69.5	4.4	20	67.44	1.52	2	-	-	-	-	-	-
02SL12	39.44019	116.00583	2660	Cpm[1]	quartzite	HFS and DTF	62.1	4.6	16	63.89	1.32	2	-	-	-	-	-	-
03SL12	39.45361	116.05631	2325	Oe[2]	quartzite	RBDS	-	-	-	76.02	1.48	2	-	-	-	-	-	-
04SL12	39.45497	116.05592	2330	Oe[2]	quartzite	RBDS	-	-	-	69.97	1.78	1	-	-	-	-	-	-
05SL12	39.42658	116.07169	2335	Oe[2]	quartzite	RBDS	-	-	-	66.21	1.42	2	-	-	-	-	-	-
06SL12	39.42836	116.08289	2275	Oe[2]	quartzite	RBDS	-	-	-	69.43	1.14	3	-	-	-	-	-	-
08SL12	39.45969	115.93231	2350	Dbpq[3]	quartzite	PSF	-	-	-	473.3	8.0	3	-	-	-	-	-	-
09SL12	39.40369	115.91289	2050	Dbpq[3]	quartzite	PSF	-	-	-	397.4	7.0	3	-	-	-	-	-	-

Footnotes:

[1]Cpm = Lower Cambrian Prospect Mountain Quartzite; [2]Oe = Middle Ordovician Eureka Quartzite; [3]Dbpq = basal quartzite of Lower Devonian Beacon Peak Dolomite

Structure abbreviations:

HFS = Hoosac fault system, RBDS = Reese and Berry detachment system, DTF = Dugout Tunnel fault, PSF = Pinto Summit fault

Section SM2: Methods and supporting data for fission-track analyses

Analyses on zircon separated from samples 01SL10, 02SL10, 06SL11, 07SL11, 01SL12, and 02SL12, and on apatite separated from sample 02SL10, were performed at the University of Arizona Fission-Track Lab by S. Thomson. Supporting data are shown in Table SM2 (single-grain data tables for individual samples are available upon request from the corresponding author). Apatite grains were mounted in epoxy resin, alumina and diamond polished, and spontaneous fission tracks were revealed by etching with 5.5M HNO_3 at 20°C for 20 seconds. Zircon grains were mounted in PFA Teflon, diamond polished, and etched in an oven at ca. 220°C using a KOH-NaOH eutectic melt (Gleadow et al., 1976) in a zirconium crucible for 3 to 50+ hours. The optimum etch time is dependent on age and radiation damage, and is monitored by repeated etching and observation at 3-6 hour time intervals. Samples were analyzed by applying the external detector method (Gleadow, 1981) using very low uranium, annealed muscovite mica detectors, and irradiated at the Oregon State University Triga Reactor, Corvallis, U.S.A. The neutron fluence was monitored using European Institute for Reference Materials and Measurements (IRMM) uranium-dosed glasses IRMM 540R for apatite and IRMM 541 for zircon. After irradiation, induced tracks in the mica external detectors were revealed by etching with 40-48% HF for 18 minutes. Spontaneous and induced FT densities were counted using an Olympus BX61 microscope at 1250x magnification with an automated Kinetek Stage system. Apatite FT lengths and Dpar values were measured using FTStage software, and an attached drawing tube and digitizing tablet supplied by T. Dumitru of Stanford University calibrated against a stage micrometer. Central ages (Galbraith and Laslett, 1993; Galbraith, 2005), quoted with 1σ errors, are calculated using the IUGS recommended zeta-calibration approach of Hurford and Green (1983). Current apatite and zircon IRMM 540R and IRMM541 zeta calibration factors of 368.1 ± 14.9 and 121.3 ± 2.6 respectively, have been obtained by repeated calibration against a number of internationally-agreed age standards including Durango and Fish Canyon apatite, and Fish Canyon and Buluk zircon, according to the recommendations of Hurford (1990).

Analyses on apatite separated from sample 06SL11 were performed at Occidental College by A. Blythe; supporting data are shown in Table SM2. Apatites were mounted in epoxy, sample surfaces were ground and polished, and apatite mounts were etched in 5.5M HNO_3 at 18°C for 22 seconds. An "external detector" (e.g., Naeser, 1979), consisting of low-U (<5 ppb) Brazil Ruby muscovite, was used for each sample. Samples were irradiated in the Oregon State Triga nuclear reactor. Following irradiation, the muscovites were etched in 48% HF at 18°C for 30 minutes. Tracks were counted using a 100X dry lens and 1250X total magnification in crystals with well-etched, clearly visible tracks and sharp polishing scratches. A Kinetek stage and software written by Dumitru (1993) were used for analyses. Standard and induced track densities were determined on external detectors (geometry factor = 0.5), and fossil track densities were determined on internal mineral surfaces. Ages were calculated using zeta 359 ± 10 for dosimeter CN-5 (e.g., Hurford and Green, 1983). All ages are central ages, with the conventional method (Green, 1981) used to determine errors on sample ages. The chi-square test estimated the probability that individual grain ages for each sample belong to a single population with Poissonian distribution (Galbraith, 1981). The data were reduced with the program Binomfit (Brandon, 2002).

Table SM2: Zircon and apatite fission-track data.

A. Analyses performed at the University of Arizona

Sample No.	Mineral	No. of Crystals	Track Density (x 10^6 tr cm^{-2})			Age Dispersion	Central Age (Ma) (±1σ)
			ρ_S (N_S)	ρ_i (N_i)	ρ_d (N_d)	($P\chi^2$)	
01SL10	Zircon	16	9.317 (1276)	4.191 (574)	0.5423 (3471)	6.3% (60.3%)	**72.5±4.5**
02SL10	Zircon	10	29.59 (3011)	2.024 (206)	0.5393 (3452)	<0.01% (99.9%)	**460.5±36.6**
	Apatite	7	0.5398 (76)	2.834 (399)	1.507 (4821)	<0.01% (99.9%)	**52.6±7.0**
06SL11	Zircon	20	5.885 (1194)	1.513 (307)	0.3203 (2050)	0.36% (76.9%)	**75.0±5.5**
07SL11	Zircon	20	6.521 (1732)	1.615 (429)	0.3193 (2043)	<0.01% (99.5%)	**77.6±5.1**
01SL12	Zircon	20	6.727 (1722)	1.855 (475)	0.3182 (2037)	0.02% (83.7%)	**69.5±4.4**
02SL12	Zircon	16	4.547 (1036)	1.400 (319)	0.3172 (2030)	<0.01% (99.6%)	**62.1±4.6**

Notes:
(i). Analyses by external detector method using 0.5 for the $4\pi/2\pi$ geometry correction factor.
(ii). Ages calculated using dosimeter glass: IRMM540R with ζ_{540R} = 368.1±14.9 (apatite); IRMM541 with ζ_{541} = 121.1±3.5 (zircon).
(iii). $P\chi^2$ is the probability of obtaining a χ^2 value for v degrees of freedom where v = no. of crystals − 1.

B. Analyses performed at Occidental College

Sample	Mineral	# grains	Standard track density x10^6 cm^{-2} (# counted)	Fossil track density x10^5 cm^{-2} (# counted)	Induced track density x10^6 cm^{-2} (# counted)	Chi square prob. %	Dpar in mm	Central age (Ma) (95% CI)	Mean Length in mm (# measured)
06SL11	Apatite	19	1.39 (4043)	2.64 (170)	1.56 (1009)	8	2.04	41.8 (+7.9/-6.7)	9.18 (1)

Section SM3: Methods and supporting data for (U-Th)/He analyses

(U-Th)/He dating of zircons separated from all twelve quartzite samples, and of apatite separated from sample 02SL10, was performed at the University of Arizona Radiogenic Helium Dating Laboratory. (U-Th)/He analyses followed the general procedures outlined in Reiners et al. (2004) and Reiners (2005) (also see laboratory website for further discussion of methods: www.geo.arizona.edu/~reiners/arhdl/arhdl.htm). Individual zircon grains were selected from separates on the basis of size, morphology, and lack of inclusions. Grains lacking obvious fractures and with a minimum radius of 60 μm, with minimal to no inclusions, were selected. The dimensions of individual grains were measured from digital photomicrographs, using the approach outlined in Hourigan et al. (2005) for alpha-ejection corrections. Single grains were then packed into 1-mm Nb foil envelopes. Multiple foil packets were then placed in individual holes in a 30-hole planchett inside a ~7-cm laser cell pumped to $<10^{-9}$ torr. Individual packets were then heated for 15 minutes by a focused beam of a 1-2 W laser, to extract ^{4}He. The packets were then re-heated for 15 minutes, often multiple times, until ^{4}He yields were less than 1% of total. Standards of Fish Canyon Tuff zircon (28.48±0.06 Ma (2σ), Schmitz and Bowring, 2001) were analyzed between every 5 unknowns.

Gas released from heated samples was spiked with 0.1-0.2 pmol ^{3}He, and condensed onto activated charcoal at the cold head of a cryogenic trap at 16 K. Helium was then released from the cold head at 37 K into a small volume (~50 cc) with an activated Zr-Ti alloy getter and the source of a Balzers quadrupole mass spectrometer (QMS) with a Channeltron electron multiplier. Peak-centered masses at approximately m/z of 1, 3, 4, and 5.2 were measured. Mass 5.2 establishes background, and mass 1 is used to correct mass 3 for HD and H3+. Corrected ratios of masses 4 to 3 were regressed through ten measurement cycles over ~15 seconds to derive an intercept value, which has an uncertainty of 0.05-0.5% over a ^{4}He/^{3}He range of ~10^{3}, and compared with the mean corrected ratio to check for significant anomalous changes in the ratio during analysis. Helium contents of unknown samples were calculated by first subtracting the average mass-1-corrected ^{4}He/^{3}He measured on multiple procedural blanks analyzed by the same method, from the mass-1-corrected ^{4}He/^{3}He measured on the unknown. This was then ratioed to the mass-1-corrected ^{4}He/^{3}He measured on a shot of an online reference ^{4}He standard analyzed with the same procedure. The resulting ratio of measured ^{4}He/^{3}He values was then multiplied by the moles of ^{4}He delivered in the reference shot.

After He extraction and measurement, foil packets were retrieved, transferred to Teflon vials, and spiked with 0.5-1.0 ng of ^{233}U and ^{229}Th. High-pressure digestion vessels were used for dissolution of the zircon and Nb foil packet. Natural-to-spike isotope ratios of U and Th were then measured on a high-resolution (single-collector) Element2 ICP-MS with all-PFA Teflon sample introduction equipment and sample preparation/analytical equipment. Blanks for zircon analyses were 2.6±0.5 pg U and 5.5±1.0 pg Th. Precision on measured U-Th ratios is typically better than 0.5% for zircon analyses. Propagated analytical uncertainties for typical zircon samples lead to an estimated analytical uncertainty on (U-Th)/He ages of approximately 1-3% (1σ). In some cases, reproducibility of multiple aliquots approaches analytical uncertainty. However, in general, reproducibility of repeat analyses of (U-Th)/He ages is significantly worse than analytical precision. Thus (U-Th)/He ages typically show a much greater scatter and higher MSWD than expected based on analytical precision alone, and multiple replicate analyses of (U-Th)/He ages on several aliquots is necessary for confidence in a particular sample age. Single-grain ZHe and AHe ages and supporting data are shown on Tables SM3 and SM4, and weighted mean ages are shown on Table SM1 and on Figure 2 in the text. Single-grain ages are reported with 2σ formal analytical precision, and weighted mean ages are reported with 2σ standard error.

Table SM3: Single grain zircon (U-Th)/He ages and supporting data.

Sample name	pmol He	1σ ± pmol He	ng U	1σ ± ng U	ng Th	1σ ± ng Th	Th/U	raw age (Ma)	2σ ± raw age (Ma)	Ft ^{238}U	Ft ^{235}U	Ft ^{232}Th	half-width (μm)	ppm U (morph)	1σ ± ppm U (morph)	ppm Th (morph)	1σ ± ppm Th (morph)	nmol ^{4}He/g (morph)	1σ ± nmol ^{4}He/g (morph)	corrected age (Ma)	2σ ± corrected age (Ma)
01SL10_z1	0.20	0.00	0.56	0.01	0.53	0.01	0.97	53.98	1.57	0.71	0.67	0.67	40.28	183.60	2.63	173.92	2.83	65.66	0.57	77.25	2.27
01SL10_z2	0.16	0.00	0.44	0.01	0.57	0.01	1.33	50.36	1.50	0.77	0.73	0.73	52.03	72.25	1.06	93.40	1.41	25.71	0.24	66.28	1.98
01SL10_z3	0.72	0.01	1.73	0.03	2.06	0.03	1.22	60.00	1.82	0.79	0.76	0.76	58.60	218.02	3.16	258.53	4.16	90.71	0.90	76.37	2.33
weighted mean																				72.57	1.26
02SL10_z2	0.25	0.00	0.67	0.01	0.37	0.01	0.56	62.01	2.00	0.79	0.76	0.76	58.96	153.07	2.22	83.98	1.32	58.08	0.59	85.33	2.54
02SL10_z3	0.77	0.01	1.87	0.03	0.75	0.01	0.41	69.66	2.34	0.82	0.79	0.79	67.67	283.26	4.54	113.40	1.81	117.07	1.04	78.50	2.88
weighted mean																				81.50	1.90
06SL11_z1	0.18	0.00	0.14	0.00	0.07	0.00	0.49	207.47	5.78	0.75	0.72	0.72	48.36	38.40	0.55	18.47	0.41	48.68	0.25	276.18	7.78
06SL11_z2	1.23	0.01	0.76	0.01	0.46	0.01	0.62	257.10	7.37	0.72	0.68	0.68	41.96	323.13	5.06	196.32	2.85	523.39	2.32	358.62	10.44
weighted mean																				305.6	6.2
07SL11_z1	0.53	0.00	1.69	0.03	0.78	0.78	0.01	52.26	1.56	0.81	0.78	0.78	63.90	188.10	2.95	86.18	1.35	58.96	0.34	64.87	1.95
07SL11_z2	0.24	0.00	0.82	0.01	0.39	0.39	0.01	48.39	1.32	0.75	0.72	0.72	48.22	182.03	2.59	85.76	1.38	52.96	0.29	64.77	1.78
07SL11_z3	0.09	0.00	0.31	0.01	0.21	0.21	0.00	46.60	1.42	0.78	0.75	0.75	55.34	58.61	0.94	38.69	0.61	17.08	0.12	60.03	1.84
weighted mean																				63.20	1.06
01SL12_z1	0.82	0.01	1.98	0.03	0.78	0.01	0.40	70.32	2.11	0.72	0.69	0.69	43.14	659.83	9.98	258.66	3.74	274.79	1.80	97.52	2.94
01SL12_z3	0.17	0.00	0.64	0.01	0.45	0.01	0.71	41.05	1.29	0.73	0.70	0.70	44.80	240.80	4.07	166.82	2.49	62.20	0.41	56.41	1.78
weighted mean																				67.44	1.52
02SL12_z1	0.25	0.00	0.86	0.01	0.49	0.01	0.59	46.92	1.46	0.77	0.74	0.74	53.17	165.10	2.36	94.39	1.37	47.57	0.45	61.07	1.91
02SL12_z3	0.22	0.00	0.64	0.01	0.57	0.01	0.92	53.66	1.48	0.81	0.78	0.78	64.94	74.67	1.06	67.32	0.97	26.31	0.19	66.54	1.84
weighted mean																				63.89	1.32
03SL12_z1	0.22	0.00	0.62	0.01	0.59	0.01	0.98	52.94	1.41	0.78	0.75	0.75	55.18	142.62	2.04	136.50	1.98	50.11	0.33	68.37	1.84
03SL12_z2	0.16	0.00	0.36	0.01	0.24	0.00	0.69	69.79	1.93	0.78	0.74	0.74	54.18	96.91	1.38	64.93	1.24	42.46	0.27	90.37	2.51
weighted mean																				76.02	1.48
04SL12_z2	0.19	0.00	0.55	0.01	0.41	0.01	0.76	54.05	1.37	0.78	0.75	0.75	54.42	131.10	1.86	96.96	1.40	45.06	0.19	69.97	1.78
weighted mean																				69.97	1.78
05SL12_z2	0.41	0.00	1.29	0.02	0.51	0.01	0.40	53.51	1.41	0.80	0.77	0.77	60.61	273.38	3.89	107.08	1.55	86.50	0.33	67.21	1.78
05SL12_z3	0.14	0.00	0.46	0.01	0.27	0.00	0.60	50.71	1.87	0.79	0.76	0.76	58.30	98.95	1.41	58.15	0.87	30.93	0.42	64.41	2.38
weighted mean																				66.21	1.42
06SL12_z1	0.22	0.00	0.66	0.01	0.33	0.00	0.50	54.99	1.52	0.69	0.65	0.65	37.75	424.63	6.03	208.85	3.06	141.10	0.87	80.40	2.24
06SL12_z2	0.21	0.00	0.64	0.01	0.30	0.00	0.48	54.35	1.76	0.76	0.73	0.73	51.12	203.41	2.91	95.66	1.38	66.49	0.68	71.46	2.32
06SL12_z3	0.63	0.00	1.91	0.03	1.37	0.02	0.74	51.95	1.32	0.83	0.80	0.80	72.48	202.03	2.87	145.00	2.11	66.43	0.29	62.87	1.61
weighted mean																				69.43	1.14
08SL12_z1	0.91	0.00	0.34	0.00	0.14	0.00	0.43	431.67	12.17	0.79	0.76	0.76	59.43	39.18	0.56	16.49	0.25	104.12	0.53	540.23	15.44
08SL12_z2	1.59	0.01	0.78	0.01	0.62	0.01	0.81	308.62	8.46	0.81	0.78	0.78	63.85	149.86	2.13	118.38	1.71	303.57	1.94	381.95	10.58
08SL12_z3	1.70	0.01	0.49	0.01	0.24	0.00	0.49	546.16	15.69	0.78	0.75	0.75	55.40	141.78	2.03	67.93	0.99	487.75	2.77	693.67	20.29
weighted mean																				473.3	8.0
09SL12_z1	0.36	0.00	0.22	0.00	0.11	0.00	0.53	261.94	7.51	0.72	0.68	0.68	41.73	135.19	1.93	69.34	1.06	218.88	1.46	365.65	10.64
09SL12_z2	1.49	0.01	0.42	0.01	0.15	0.00	0.37	579.45	17.08	0.77	0.74	0.74	53.65	131.89	1.92	47.99	0.73	471.44	2.52	740.60	22.25
09SL12_z3	0.46	0.00	0.28	0.00	0.09	0.00	0.34	275.45	7.78	0.77	0.74	0.74	53.59	86.57	1.24	28.85	0.43	142.04	0.71	354.92	10.13
weighted mean																				397.40	7.00

Notes:

1. Ft is alpha ejection correction (Reiners, 2005).
2. Singe-grain ages are reported with 2σ formal analytical precision.
3. Weighted mean ages are reported with 2σ standard error, calculated from Isoplot, version 4.1 (Ludwig, 2008).
4. Half-width is c-axis perpendicular half-width.

Table SM4: Single grain apatite (U-Th)/He ages and supporting data.

Sample name	pmol He	1σ ± pmol He	ng U	1σ ± ng U	ng Th	1σ ± ng Th	Th/U	raw age (Ma)	2σ ± raw age (Ma)	Ft ^{238}U	Ft ^{235}U	Ft ^{232}Th	Ft ^{147}Sm	half-width (μm)	ppm U (morph)	1σ ± ppm U (morph)	ppm Th (morph)	1σ ± ppm Th (morph)	nmol ^{4}He/g (morph)	1σ ± nmol ^{4}He/g (morph)	corrected age (Ma)	2σ ± corrected age (Ma)
02SL10_a1	0.01	0.00	0.05	0.00	0.01	0.00	0.12	22.81	0.42	0.77	0.73	0.73	0.92	61.30	8.98	0.14	1.03	0.02	1.14	0.01	29.85	1.10
02SL10_a3	0.00	0.00	0.01	0.00	0.02	0.00	4.52	15.31	0.48	0.60	0.55	0.55	0.87	34.02	6.71	0.14	29.54	0.43	1.15	0.03	26.51	1.65
weighted mean																					28.82	0.92

Notes:
1. Ft is alpha ejection correction (Reiners, 2005).
2. Singe-grain ages are reported with 2σ formal analytical precision.
3. Weighted mean ages are reported with 2σ standard error, calculated from Isoplot, version 4.1 (Ludwig, 2008).
4. Half-width is c-axis perpendicular half-width.

Section SM4: Supporting information for time-temperature path modeling

(U-Th)/He and fission-track ages, along with temperature ranges estimated from integrating depth measurements on the cross-sections with bracketing constraints on geothermal gradient in the study area, were used to inverse-model time-temperature (t-T) paths for 10 samples using the HeFTy program (Ketcham, 2005). The following section describes methods for estimating t-T constraints input into the thermal models, and modeling parameters.

Depth constraints for individual samples were measured from the restored and deformed cross-sections (Fig. 2C in the text), and are summarized in Table SM5. The vertical depth below the top of the Pennsylvanian-Permian unit (IPP) after the Early Cretaceous (ca. 122-116 Ma; Long et al., 2014) construction of the Eureka culmination is a first-order estimate of the maximum structural burial depth that each sample attained. Regionally, no Paleozoic or early Mesozoic rock units stratigraphically higher than the Lower Permian Carbon Ridge Formation and laterally-equivalent Garden Valley Formation are observed (Roberts et al., 1967; Hose and Blake, 1976). Also, on the basis of westward onlap of Triassic rocks and westward erosional truncation of Permian rocks below Triassic rocks, several studies have argued that central Nevada was a topographic high during much of the Triassic (Burchfiel et al., 1974; Collinson et al., 1976; Stewart, 1980), and therefore did accumulate a thick section of Triassic rocks. In addition, compilations of conodont alteration indices from Pennsylvanian, Permian, and Mississippian rocks from the study area and surrounding region are characterized by values of 1 (Harris et al., 1980; Crafford, 2007), which corresponds to a maximum burial temperature range of ca. 50-80 °C (Konigshof, 2003), indicating that rocks in the study area were not deeply buried beyond observed stratigraphic depths (Long, 2012). This is particularly important for Mississippian rocks, which were already buried as deeply as ~2.5-3.0 km based on observed Mississippian-Permian stratigraphic thicknesses (Long et al., 2014).

The minimum depth of samples prior to motion on set 1 normal faults is constrained by Mississippian and Permian rocks that are preserved in the hanging walls of the Hoosac fault system and Pinto Summit fault on both cross-sections, which restore near the culmination crest (Fig. 2C in the text). This depth, together with the measured depth below the top of the Pennsylvanian-Permian section, constrains the permissible range of pre-extensional erosional exhumation of the culmination crest zone to ~0.5-2.2 km. The depth of samples after motion on set 1 normal faults and prior to motion on set 2 normal faults was measured, which allowed estimation of tectonic exhumation accompanying motion on set 1 faults. Similarly, measurement of the depth of samples after motion on set 2 normal faults allowed estimation of tectonic exhumation accompanying motion on set 2 faults, and estimation of post-set 2 exhumation that brought samples to the modern surface.

Maximum and minimum constraints were placed on the past geothermal gradient in the study area, by integrating measured burial depths, ZHe and ZFT ages that have been reset and un-reset post-deposition, and estimated ranges of closure temperature for these thermochronologic systems. These constraints are summarized in Table SM6 and Figure SM1. Closure temperature ranges of 180 ± 20˚C and 205 ± 18˚C were used for

the ZHe and ZFT systems, respectively (Reiners et al., 2004; 2005; Bernet, 2009). Three samples that yielded Paleozoic ZHe ages (06SL11, 08SL12, 09SL12), and one sample that yielded a Paleozoic ZFT age (02SL10), indicate that burial temperatures did not exceed closure temperatures for these systems after deposition, and when combined with estimates of maximum burial depth, constrain the maximum permissible geothermal gradient (Table SM6; Fig. SM1A).

In addition, the 12 grains that yielded the oldest ZFT ages from sample 06SL11 show a correlation between U concentration and age (Fig. SM1B), where grains with lower U (i.e., less radiation damage) yielded progressively older ages. This suggests that several of these less-damaged grains were not fully reset at ca. 60-80 Ma, and therefore that the maximum burial temperature that this sample experienced did not significantly exceed the ZFT closure temperature range for the more radiation-damaged grains (Bernet, 2009). Also, sample 06SL11 yielded a Late Cretaceous ZFT age and a Paleozoic ZHe age; this apparent reversal is interpreted as the result of high degrees of radiation damage in the detrital zircons analyzed, which are from a Lower Cambrian sandstone. High radiation damage has been shown to increase the ZHe closure temperature range (Guenthner et al., 2013), and has in some cases been shown to reduce the ZFT closure temperature range (e.g., Marsellos and Garver, 2010). Also, the published closure temperature ranges for the two techniques utilized here partially overlap within error.

Finally, two groups of samples that yielded Late Cretaceous to Paleocene ZFT and ZHe ages, indicating thermal resetting of these systems after deposition, were combined with burial depth measurements to constrain the minimum permissible geothermal gradient (Table SM6; Fig. SM1A). The geothermal gradient range that is compatible with all maximum and minimum bracketing constraints is 27-33˚C/km (Fig. SM1A).

The estimated geothermal gradient range was then integrated with depth measurements in order to calculate burial temperature ranges prior to motion on set 1 faults, after motion on set 1 faults, and after motion on set 2 faults (Table SM5; Figs. SM2, SM3). The temperature range prior to motion on set 1 faults was used as the starting temperature range for each individual model, at ca. 116-122 Ma, the estimated time of construction of the Eureka culmination (Long et al., 2014). In addition, all samples were modeled to have reached 10±10°C at 0 Ma.

The t-T paths shown in Figures SM2 and SM3, and Figure 3 in the text, were generated using HeFTy version 1.8.2 (Ketcham, 2005), using the following model parameters for ZHe, AFT, and AHe data:

For the ZHe model: Calibration: “Guenthner et al., 2013 (Zircon)”; Radius: Average radius of all grains used to calculate the sample weighted mean age (Table SM3); Abraded: “0 μm” (default); Model precision: “Good”; Stopping distances: “Ketcham et al. 2011”; Alpha calculation: “Ejection”; Measured age (uncorrected): The weighted mean (U-Th)/He age of uncorrected ages (‘Raw age’ column on Table SM3 and associated 1σ error) was input here, so that the resulting corrected age is equivalent to the corrected weighted mean age for the sample; Age to report: “Corrected”; Alpha correction: “Ketcham et al. 2011”; Composition: The average U and Th concentration of all grains used to calculate the weighted mean age of the sample (Table SM3) was input here; Zoned? “No.”

For the AFT model: Annealing model: “Ketcham et al. (2007a)”; C-axis projection: “Ketcham et al. (2007b), 5.0M”; Model C axis projected lengths?: “No”; Used Cf Irradiation?: “No”; Default initial mean track length: “From Dpar (μm), 16.3 μm” (default); Length reduction in standard: “0.893” (default); Kinetic parameter: “Dpar (μm).” Each sample was modeled using a single kinetic parameter (Dpar (μm)). Zeta mode: “Traditional”; Uncertainty mode: “1 SE.”

For the AHe model: Calibration: “Shuster et al. (2006) (Do/a^2) (Apatite)”; Radius: Average radius of all grains used to calculate the sample weighted mean age (Table SM4); Abraded: “0 μm” (default); Model precision: “Good”; Stopping distances: “Ketcham et al. 2011”; Alpha calculation: “Static ejection”; Measured age (uncorrected): The weighted mean (U-Th)/He age of uncorrected ages (‘Raw age’ column on Table SM4 and associated 1σ error) was input here, so that the resulting corrected age is equivalent to the corrected weighted mean age for the sample; Age to report: “Corrected”; Alpha correction: “Ketcham et al. 2011”; Composition: The average U and Th concentration of all grains used to calculate the weighted mean age of the sample (Table SM4) was input here; Zoned? “No.”

For ZFT data, the calibration options available in HeFTy correspond to predicted closure temperatures (at a cooling rate of 10°C/Myr) between ca. 280-325˚C, which are characteristic of zircons with zero radiation damage (Rahn et al., 2004; Yamada et al., 2007). Therefore, because this study analyzed detrital zircon grains from a Cambrian rock unit, which must have some degree of radiation damage, ZFT dates were entered into HeFTy as constraints in t-T space that the cooling path must pass through, rather than input as thermochronologic ages. The full closure temperature range of 187-223˚C, calibrated from a recent field-based study (Bernet, 2009), which is characteristic of natural, radiation-damaged zircons (e.g., Brandon et al., 1998), was used along with the age and error range of individual ZFT dates to define the area in t-T space that the cooling path had to pass through.

Inverse modeling for each sample used the following parameters: Search Method: "Monte Carlo" (default); Subsegment spacing: "Random" (default); Ending condition: "Paths tried = 10000" (default); Result to display: "Paths"; Merit value for 'good' fit: "0.5" (default); Merit value for 'acceptable fit' = "0.05" (default). Segments: "monotonic consistent" (default); Randomizer style: "Episodic" (default).

Table SM5: Depth measurements and burial temperature estimates for Eureka thermochronology samples.

sample	cross-section	structural depth below top IPP* (km)	pre-set 1 depth (km)	pre-set 1 erosion (km)	post-set 1 depth (km)	set 1 tectonic exhumation (km)	post-set 2 depth (km)	set 2 tectonic exhumation (km)	pre-set 1 burial temp. range (˚C)**	post-set 1 burial temp. range (˚C)**	post-set 2 burial temp. range (˚C)**
02SL10	A-A'	7.1	6.6-7.1	0.0-0.5	4.3	2.3-2.8	2.3	2.0	192-234	116-142	62-76
06SL11	A-A'	6.9	6.1-6.9	0.0-0.8	4.5	1.6-2.4	1.8	2.7	186-228	122-149	49-59
07SL11	A-A'	7.1	6.2-7.1	0.0-0.9	4.7	1.5-2.4	1.8	2.9	192-234	127-155	49-59
range	A-A'	6.9-7.1	6.1-7.1	0.0-0.9	4.3-4.7	1.5-2.8	1.8-2.3	2.0-2.9	186-234	116-155	49-76
01SL10	B-B'	8.0	5.8-8.0	0.0-2.2	4.8	1.0-3.2	2.3-2.5	2.3-2.5	216-264	130-158	62-83
01SL12	B-B'	8.0	5.9-8.0	0.0-2.1	4.9	1.0-3.1	2.3-2.4	2.5-2.6	216-264	132-162	62-79
02SL12	B-B'	8.0	6.0-8.0	0.0-2.0	4.9	1.1-3.1	2.3-2.4	2.5-2.6	216-264	132-162	62-79
range	B-B'	8.0	5.8-8.0	0.0-2.2	4.8-4.9	1.0-3.2	2.3-2.5	2.3-2.6	186-264	103-162	62-83
03SL12	A-A'	4.9	4.9	-	2.1	2.8	-	-	132-162	57-69	-
04SL12	A-A'	4.9	4.9	-	2.3	2.6	-	-	132-162	62-76	-
range	A-A'	4.9	4.9	-	2.1-2.3	2.6-2.8	-	-	132-162	57-76	-
05SL12	B-B'	5.9	5.9	-	3.9	2.0	-	-	159-195	105-129	-
06SL12	B-B'	5.4	5.4	-	4.1	1.3	-	-	146-178	111-135	-
range	B-B'	5.4-5.9	5.4-5.9	-	3.9-4.1	1.3-2.0	-	-	146-195	105-135	-
08SL12	A-A'	4.3	3.8-4.3	-	-	-	1.5	2.3-2.8	116-142	-	41-50
09SL12	C-C'***	4.5	4.0-4.5	-	-	-	4.0	0.0-0.5	122-149	-	108-132
range	-	4.3-4.5	3.8-4.5	-	-	-	1.5-4.0	0.0-2.8	116-149		41-132

Footnotes:

*IPP stands for the Pennsylvanian-Permian map unit shown on Figure 2 in the text.

**Estimated using the 30±3˚C/km bracketed geothermal gradient range for the study area; see supporting data in Table SM6 and Figure SM1.

***Cross-section C-C' is published in Long et al. (2014).

Table SM6: Data bracketing geothermal gradient (dT/dz) in the study area.

sample(s)	08SL12 09SL12	06SL11	02SL10	01SL10 06SL11 07SL11 01SL12 02SL12	03SL12 04SL12 05SL12 06SL12
footwall of structure	PSF	HFS and DTF	HFS and DTF	HFS and DTF	RBDS
system	ZHe (un-reset)	ZHe (un-reset)	ZFT (un-reset)	ZFT (reset)	ZHe (reset)
max. or min. dT/dz	maximum	maximum	maximum	minimum	minimum
min. depth (km)	3.8	6.1	6.6	5.8	4.9
max. depth (km)	4.5	6.9	7.1	8.0	5.9
low Tc (˚C)*	160	160	187	187	160
high Tc (˚C)*	200	200	223	223	200
low dT/dz (˚C/km)	36	23	26	23	27
high dT/dz (˚C/km)	53	33	34	38	41

Footnotes:
*Tc = closure temperature range; 160-200˚C for ZHe from Reiners (2005); 187-223˚C for ZFT from Bernet (2009).

Structure abbreviations:
PSF = Pinto Summit fault; HFS = Hoosac fault system; DTF = Dugout Tunnel fault; RBDS = Reese and Berry detachment system.

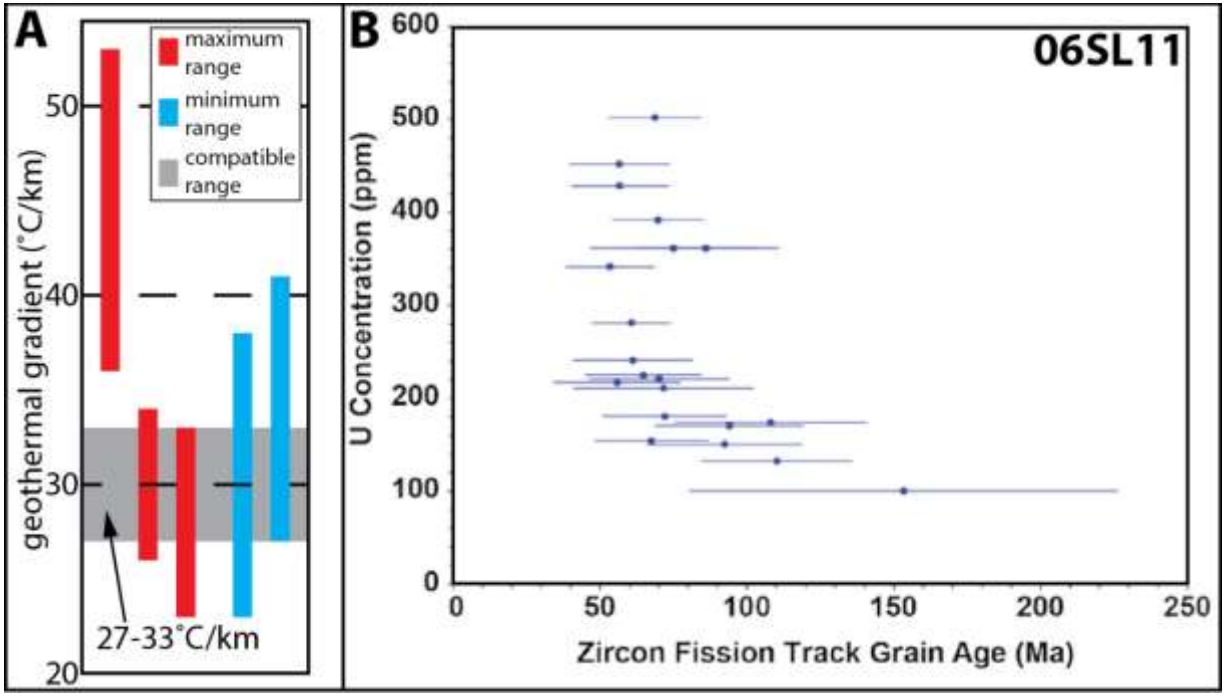

Figure SM1: A) Graph of constraints bracketing geothermal gradient in study area (see Table SM6 for supporting data). Red bars plot maximum permissible geothermal gradient ranges, and blue bars plot minimum ranges. Gray shaded area (27-33˚C/km) represents geothermal gradient range compatible with all constraints. B) Graph of U concentration versus ZFT age for individual grains analyzed from sample 06SL11, showing a correlation between grain age and U concentration for the oldest twelve grains.

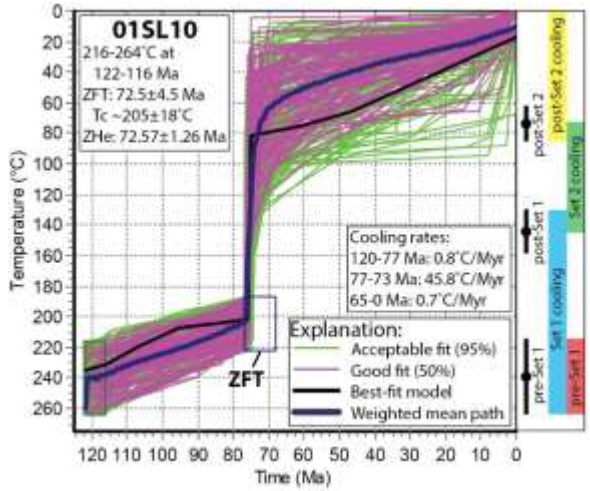
01SL10
216-264°C at
122-116 Ma
ZFT: 72.5±4.5 Ma
Tc ~205±18°C
ZHe: 72.57±1.26 Ma
Cooling rates:
120-77 Ma: 0.8°C/Myr
77-73 Ma: 45.8°C/Myr
65-0 Ma: 0.7°C/Myr
Explanation:
Acceptable fit (95%)
Good fit (50%)
Best-fit model
Weighted mean path
ZFT
Temperature (°C)
Time (Ma)
post-Set 2
post-Set 1
pre-Set 1
post-Set 2 cooling
Set 2 cooling
Set 1 cooling
pre-Set 1

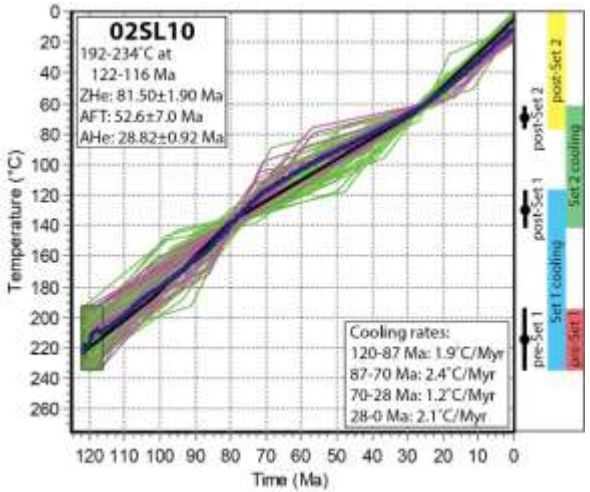
02SL10
192-234°C at
122-116 Ma
ZHe: 81.50±1.90 Ma
AFT: 52.6±7.0 Ma
AHe: 28.82±0.92 Ma
Cooling rates:
120-87 Ma: 1.9°C/Myr
87-70 Ma: 2.4°C/Myr
70-28 Ma: 1.2°C/Myr
28-0 Ma: 2.1°C/Myr
Temperature (°C)
Time (Ma)
post-Set 2
post-Set 1
pre-Set 1
Set 2 cooling
Set 1 cooling
pre-Set 1

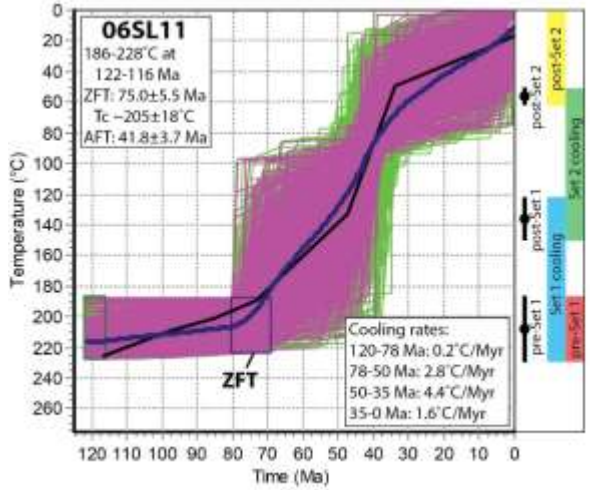
06SL11
186-228°C at
122-116 Ma
ZFT: 75.0±5.5 Ma
Tc ~205±18°C
AFT: 41.8±3.7 Ma
Cooling rates:
120-78 Ma: 0.2°C/Myr
78-50 Ma: 2.8°C/Myr
50-35 Ma: 4.4°C/Myr
35-0 Ma: 1.6°C/Myr
ZFT
Temperature (°C)
Time (Ma)
post-Set 2
post-Set 1
pre-Set 1
Set 2 cooling
Set 1 cooling
pre-Set 1

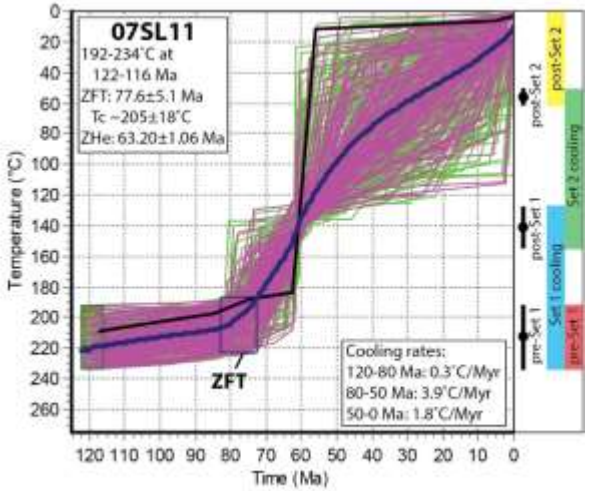
07SL11
192-234°C at
122-116 Ma
ZFT: 77.6±5.1 Ma
Tc ~205±18°C
ZHe: 63.20±1.06 Ma
Cooling rates:
120-80 Ma: 0.3°C/Myr
80-50 Ma: 3.9°C/Myr
50-0 Ma: 1.8°C/Myr
ZFT
Temperature (°C)
Time (Ma)
post-Set 2
post-Set 1
pre-Set 1
Set 2 cooling
Set 1 cooling
pre-Set

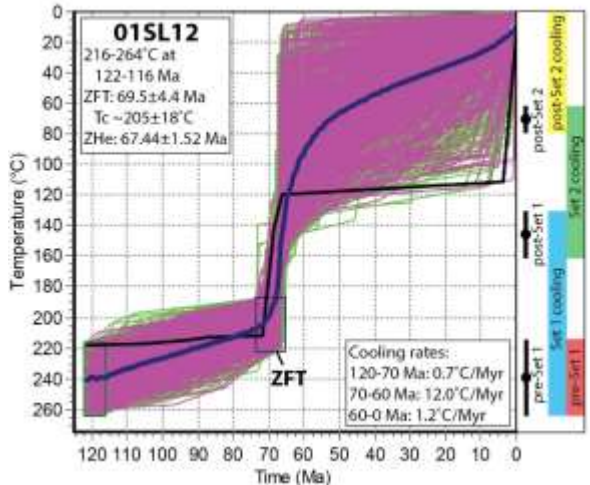
01SL12
216-264°C at
122-116 Ma
ZFT: 69.5±4.4 Ma
Tc ~205±18°C
ZHe: 67.44±1.52 Ma
Cooling rates:
120-70 Ma: 0.7°C/Myr
70-60 Ma: 12.0°C/Myr
60-0 Ma: 1.2°C/Myr
ZFT
Temperature (°C)
Time (Ma)
post-Set 2
post-Set 1
pre-Set 1
post-Set 2 cooling
Set 2 cooling
Set 1 cooling
pre-Set 1

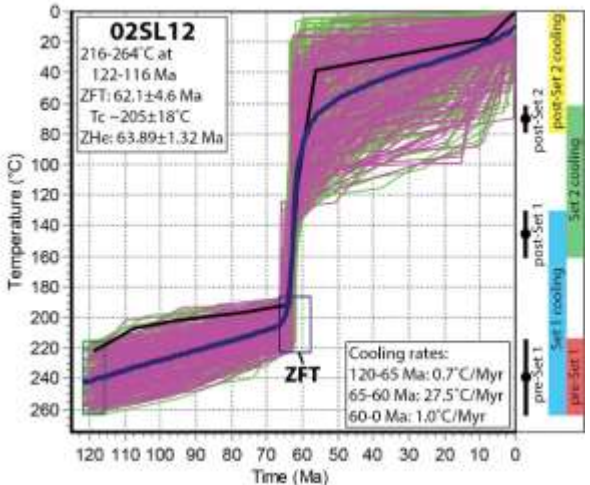
02SL12
216-264°C at
122-116 Ma
ZFT: 62.1±4.6 Ma
Tc ~205±18°C
ZHe: 63.89±1.32 Ma
Cooling rates:
120-65 Ma: 0.7°C/Myr
65-60 Ma: 27.5°C/Myr
60-0 Ma: 1.0°C/Myr
ZFT
Temperature (°C)
Time (Ma)
post-Set 2
post-Set 1
pre-Set 1
post-Set 2 cooling
Set 2 cooling
Set 1 cooling
pre-Set 1

Figure SM2: Modeled t-T paths for Cambrian quartzite samples in the footwall of the Hoosac fault system (set 1) and Dugout Tunnel fault (set 2). Burial temperature ranges and cooling ranges before and after motion on set 1 and set 2 normal faults (Table SM5) are plotted to the right of each graph. Cooling rates from weighted mean paths are shown.

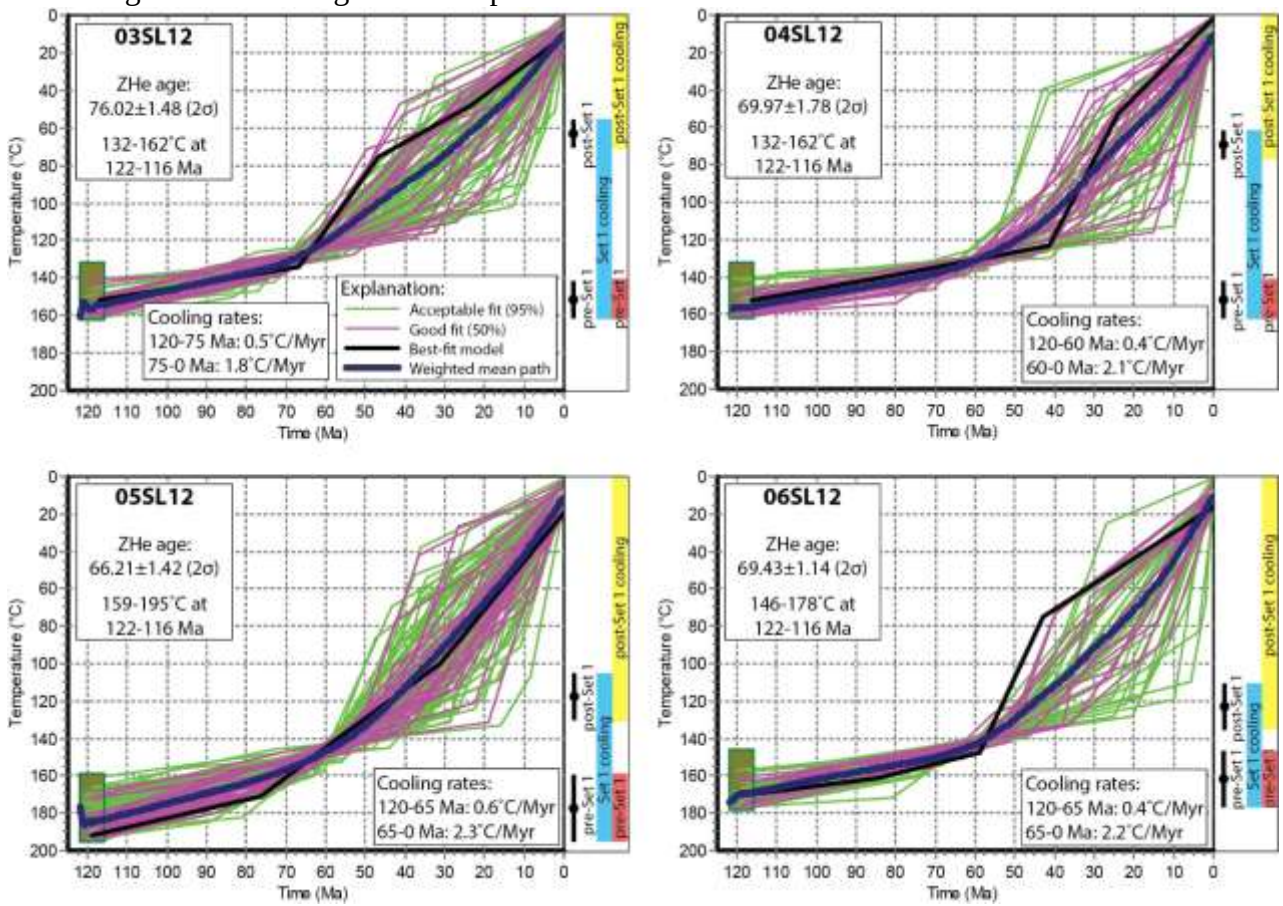

Figure SM3: Modeled t-T paths for Ordovician quartzite samples in the footwall of the Reese and Berry detachment system (set 1). Burial temperature ranges and cooling ranges before and after motion on set 1 normal faults (Table SM5) are plotted to the right of each graph. Cooling rates from weighted mean paths are shown.

References cited

Bernet, M., 2009, A field-based estimate of the zircon fission-track closure temperature: Chemical Geology, v. 259, p. 181-189, doi.org/10.1016/j.chemgeo.2008.10.043.

Brandon, M.T., 2002, On Track, v. 24, p. 13-18.

Brandon, M.T., Roden-Tice, M.K., and Garver, J.I., 1998, Late Cenozoic exhumation of the Casdacia accretionary wedge in the Olympic Mountains, northwest Washington State: Geological Society of America Bulletin, v. 110, p. 985-1009.

Burchfiel, B.C., Fleck, R.J., Secor, D.T., Vincelette, R.R., and Davis, G.A., 1974, Geology of the Spring Mountains, Nevada: Geological Society of America Bulletin, v. 85, p. 1013-1022.

Collinson, J.W., Kendall, C.G., and Marcantel, J.B., 1976, Permian-Triassic boundary in eastern Nevada and west-central Utah: Geological Society of America Bulletin, v. 87, p. 821-824.

Crafford, A.E.J., 2007, Geologic Map of Nevada: U.S. Geological Survey Data Series 249, 1 CD-ROM, 46 p., 1 plate.

Dumitru, T.A., 1993, A new computer automated microscope stage system for fission-track analysis: Nuclear Tracks and Radiation Measurements, v. 21, p. 575–580.

Galbraith, R.F., 1981, On statistical methods of fission track counts: Mathematical Geology, v. 13, p. 471–478.

Galbraith, R.F., 2005, Statistics for Fission Track Analysis, Chapman & Hall/CRC, Boca Raton, 219 pp.

Galbraith, R.F., and Laslett, G.M., 1993, Statistical models for mixed fission track ages: Nuclear Tracks, v. 21, 459-470.

Gleadow, A.J.W., 1981, Fission-track dating methods: what are the real alternatives?: Nuclear Tracks, v. 5, p. 3-14.

Gleadow, A.J.W., Hurford, A.J. and Quaife, R.D., 1976, Fission track dating of zircon: improved etching techniques: Earth and Planetary Science Letters, v. 33, p. 273-276.

Green, P.F., 1981, A new look at statistics in fission track dating: Nuclear Tracks, v. 5, p. 77–86.

Guenthner, W.R., Reiners, P.W., Ketcham, R.A., Nasdala, L., and Geister, G., 2013, Helium diffusion in natural zircon: Radiation damage, anisotropy, and the interpretation of zircon (U-Th)/He thermochronology: American Journal of Science, v. 313, p. 145-198, doi 10.2475/03.2013.01.

Harris, A.G., Wardlaw, B.R., Rust, C.C., and Merrill, G.K., 1980, Maps for assessing thermal maturity (conodont color alteration index maps) in Ordovician through Triassic rocks in Nevada and Utah and adjacent parts of Idaho and California: United States Geological Survey Miscellaneous Investigations Series, Map I-1249, 2 sheets.

Hose, R.K., and Blake, M.C., Jr., 1976, Geologic map of White Pine County, Nevada, USGS Open-File Report OF-70-166.

Hourigan, J.K., Reiners, P.W., and Brandon M.T., 2005, U-Th zonation-dependent alpha-ejection in (U-Th)/He chronometry: Geochimica et Cosmochimica Acta, v. 69, p. 3349-3365.

Hurford, A.J., 1990, Standardization of fission track dating calibration: Recommended by the Fission Track Working Group of the I.U.G.S. Subcommission on Geochronology: Chemical Geology, v. 80, 171-178.

Hurford, A.J., and Green, P.F., 1983, The Zeta age calibration of fission-track dating: Isotope Geoscience, v. 1, p. 285–317.

Ketcham, R.A., 2005, Forward and inverse modeling of low-temperature thermochronometry data, *in* Reiners, P.W., and Ehlers, T.A., eds., Low-Temperature Thermochronology: Techniques, Interpretations, and Applications: Reviews in Mineralogy and Geochemistry, v. 58, p. 275–314, Mineralogical Society of America, Chantilly, VA.

Ketcham, R. A., Carter, A., Donelick, R.A., Barbarand, J., and Hurford, A.J., 2007a, Improved measurement of fission-track annealing in apatite using c-axis projection: American Mineralogist, v. 92, p. 789–798, doi:10.2138/am.2007.2280.

Ketcham, R. A., Carter, A., Donelick, R.A., Barbarand, J., and Hurford, A.J., 2007b, Improved modeling of fission-track annealing in apatite: American Mineralogist, v. 92, p. 799–810, doi:10.2138/am.2007.2281.

Ketcham, R.A., Gautheron, C., and Tassan-Got, L., 2011, Accounting for long alpha-particle stopping distances in (U-Th-Sm)/He geochronology: Refinement of the baseline case: Geochimica et Cosmochimica Acta, v. 75, p. 7779-7791.

Konigshof, P., 2003, Conodont deformation patterns and textural alteration in Paleozoic conodonts: examples from Germany and France: Paleobiodiversity and Paleoenvironments, v. 83, p. 149-156.

Long, S.P., 2012, Magnitudes and spatial patterns of erosional exhumation in the Sevier hinterland, eastern Nevada and western Utah, USA: Insights from a Paleogene paleogeologic map: Geosphere, v. 8, p. 881-901, doi: 10.1130/GES00783.1.

Long, S.P., Henry, C.D., Muntean, J.L., Edmondo, G.P., and Cassel, E.J., 2014, Early Cretaceous construction of a structural culmination, Eureka, Nevada, U.S.A.: implications for out-of-sequence deformation in the Sevier hinterland: Geosphere, v. 10, p. 505-553, doi: 10.1130/GES00997.1.

Ludwig, K.J., 2008, Isoplot 3.70: Berkeley Geochronology Center Special Publication 4, 76 p.

Marsellos, A.E., and Garver, J.I., 2010, Radiation damage and uranium concentration in zircon as assessed by Raman spectroscopy and neutron irradiation: American Mineralogist, v. 95, p. 1192–1201, doi:10.2138/am.2010.3264.

Naeser, C.W., 1979, Fission track dating and geologic annealing of fission tracks: in Jager, E., and Hunziker, J.C., eds., Lectures in Isotope Geology, Springer-Verlag, Berlin, p. 154-169.

Rahn, M.K., Brandon, M.T., Batt, G.E., and Garver, J.I., 2004, A zero-damage model for fission-track annealing in zircon: American Mineralogist, v. 89, p. 473-484.

Reiners, P.W., 2005, Zircon (U-Th)/He thermochronometry: Reviews in Mineralogy and Geochemistry, v. 58, p. 151-179, doi:10.2138/rmg.2005.58.6.

Reiners, P.W., Spell, T.L., Nicolescu, S., and Zanetti K.A., 2004, Zircon (U-Th)/He thermochronometry: He diffusion and comparisons with $^{40}Ar/^{39}Ar$ dating: Geochimica et Cosmochimica Acta, v. 68, p. 1857-1887.

Reiners, P.W., and Ehlers, T.A., and Zeitler, P.K., 2005, Past, present, and future of thermochronology: Reviews in Mineralogy and Geochemistry, v. 58, p. 1-18.

Roberts, R.J., Montgomery, K.M., and Lehner, R.E., 1967, Geology and Mineral Resources of Eureka County, Nevada: Nevada Bureau of Mines and Geology Bulletin 64, 152 p., 11 plates.

Schmitz, M.D., and Bowring, S.A., 2001, U-Pb zircon and titanite systematics of the Fish Canyon Tuff: an assessment of high-precision U-Pb geochronology and its application to young volcanic rocks: Geochimica et Cosmochimica Acta, v. 65, p. 2571-2587, doi:10.1016/S0016-7037(01)00616-0.

Shuster, D.L., Flowers, R.M., and Farley, K.A., 2006, The influence of natural radiation damage on helium diffusion kinetics in apatite: Earth and Planetary Science Letters, v. 249, p. 148-161.

Stewart, J.H., 1980, Geology of Nevada: a discussion to accompany the Geologic Map of Nevada: Nevada Bureau of Mines and Geology Special Publication 4, 136 p.

Yamada, R., Murakami, M., and Tagami, T., 2007, Statistical modeling of annealing kinetics of fission tracks in zircon; Reassessment of laboratory experiments: Chemical Geology, v. 236, p. 75-91.